Ingeniería y Competitividad
Vol 28 (1) 2026 doi: 10.25100/iyc.v28i1.14980

Vol 28 (1)

ISSN
0123-3033
e- 2027-8284

Original Article

Design of Experiments to enhance spraying parameters for YSZ coatings via Atmospheric Plasma Spraying

Diseño de experimentos para mejorar los parámetros de proyección de recubrimientos de YSZ mediante proyección por plasma atmosférico

Jhonattan de la Roche[1] Alexander Arboleda[1] Lina María Chica[2] Alejandro Toro[1]

[1] Tribology and Surfaces Group, Universidad Nacional de Colombia. Medellín, Colombia
[2] GICI, Universidad de Medellín. Medellín, Colombia

Abstract

Objectives: To implement the Design of Experiments (DOE) methodology to obtain the projection parameters for the deposition of yttria-stabilized zirconia (YSZ) on Inconel 625 by atmospheric plasma spraying (APS).
Methodology:A 32 factorial design with three repetitions was implemented, in which the factors were the electrical current and the hydrogen flow rate. The response variables were the mean particle velocity and the particle temperature in flight. Coating quality was evaluated in terms of tetragonal phase content, porosity, and coating thickness.
Results: The samples deposited at 430 A and hydrogen flow rates of 7 and 9 NLPM exhibited the most outstanding characteristics. The sample deposited at 430 A and 7 NLPM of H□ was subjected to thermal shock tests.
Conclusions:The sample deposited at 430 A and 7 NLPM of H□ demonstrated superior performance compared to similar coatings reported in the scientific literature.

Keywords: YSZ coatings, APS, Spraying parameters, Design of Experiments

Resumen

Objetivos: Implementar la metodología de Diseño de Experimentos (DOE) para obtener los parámetros de proyección en la deposición de circonia estabilizada con itria (YSZ) sobre Inconel 625 mediante proyección térmica por plasma atmosférico (APS).
Metodología: Se implementó un diseño factorial 3^2 con tres repeticiones, en el cual los factores fueron la corriente eléctrica y el flujo de hidrógeno. Las variables respuesta fueron la velocidad media y la temperatura de las partículas en vuelo. La calidad de los recubrimientos se evaluó en función del porcentaje de fase tetragonal, la porosidad y el espesor.
Resultados: Las muestras depositadas entre 430 A y flujos de H□ de 7 y 9 NLPM exhibieron las características más sobresalientes. La muestra depositada a 430 A y 7 NLPM de H□ fue sometida a pruebas de choque térmico.
Conclusiones: La muestra depositada a 430 A y 7 NLPM de H□ demostró un rendimiento superior al de recubrimientos similares documentados en la literatura científica.

Palabras clave: recubrimientos de YSZ, APS, parámetros de proyección, Diseño de experimentos

How to cite?

De la Roche J, Arboleda A, Chica LM, Toro A. Design of Experiments to enhance spraying parameters for YSZ coatings via Atmospheric Plasma Spraying Ingeniería y Competitividad, 2026, 28(1)e-20114980.

https://doi.org/10.25100/iyc.v28i1.14980

Received: 16/06/25
Reviewed: 15/09/25
Accepted: 26/01/26
Online: 5/02/26

Correspondence

jdey@unal.edu.co

Spanish version

Why was this study conducted?

This study was conducted as part of a larger project with Empresas Públicas de Medellín (EPM) aimed at supporting the implementation of Atmospheric Plasma Spray (APS) technology for the repair and protection of hot gas path components in thermoelectric gas turbines. In this context, it was necessary to optimize the deposition parameters for YSZ thermal barrier coatings (TBCs) on Inconel 625, ensuring appropriate particle in-flight conditions and achieving coatings with suitable microstructural and phase characteristics for high-temperature service.

What were the most relevant findings?

The most relevant findings were that a Design of Experiments (DOE) approach successfully identified the APS spraying conditions that produced the best coating quality. The combination of 430 A and H□ flowrates within the 7–9 NLPM range resulted in coatings with favorable characteristics, including high tetragonal phase content (92.5%), controlled porosity (15.9%), and adequate thickness (225 µm). Additionally, the study established a clear relationship between in-flight particle temperature (2310–2470 °C) and velocity (150–172 m/s) and key coating outcomes such as microstructure, thickness, porosity, and crystalline phase composition. Finally, the optimized coating condition (430 A + 7 NLPM H□) demonstrated strong performance in thermal shock testing, sustaining more than 600 cycles, outperforming similar coatings reported in the literature.

What do these findings contribute?

These findings contribute a systematic and transferable methodology for APS parameter optimization, enabling researchers and industry to efficiently link process parameters and in-flight diagnostics to the final coating properties required for specific applications. The proposed DOE-based strategy provides a practical framework to design robust YSZ coatings for thermal barrier applications, supporting improved performance and reliability in high-temperature components such as gas turbine hot gas path parts.

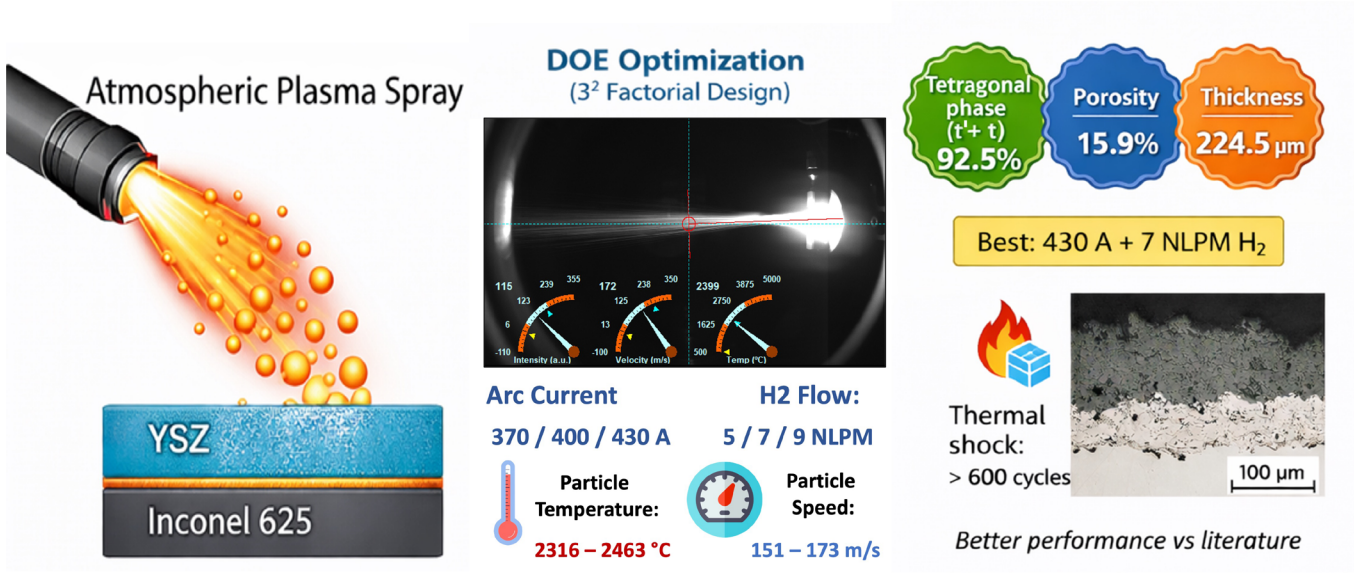

doi: 10.25100/iyc.v28i1.14980

Introduction

Power generation is a demanding industrial activity that entails a constant search for higher efficiencies and improvements of the durability of components to fulfill the requirements from the market. In the case of thermoelectric generation, the improvements implemented over the last 30 years in the design and manufacturing of critical components have allowed significant increases of the operating temperatures of the gas turbines. Among these improvements are the formulation of new alloys, progress in casting processes (components with directional and monocrystalline solidification) and the implementation of internal cooling channels in the components (1–3). However, the highest contribution to efficiency was made by incorporating thermal barrier coatings (TBCs) in components exposed to high temperatures such as the combustion chamber, liners and first stage airfoils, allowing them to operate at temperatures above the melting point of the base material (Nickel-based super alloy), which is approximately 1300°C (4,5).

A TBC is made up of 3 layers: the first one is called bond coat (BC), which is generally a MCrAlY alloy (where M=Ni, Co or Ni+Co) and is applied directly to the substrate. The second layer is the thermally grown oxide (TGO), which is formed throughout oxidation of the BC and provides higher thermal resistance, oxygen barrier and adhesion to top coat (6,7). Finally, the Top Coat (TC) is the layer in contact with the external environment at high temperatures. Yttria Stabilized Zirconia (YSZ) with concentrations between 7 and 8 wt.% by weight (4-4.5% in moles) is typically used as the TC due to its thermal and mechanical properties at high temperatures (8,9). Among the processes to deposit the TC, Atmospheric Plasma Spray (APS) is one of the most used for thermoelectric generation turbine components due to its versatility and low cost (10). Moreover, the splat-type microstructure and the intrinsic defects (pores and cracks) characteristics of the plasma spray process provides multiple desirable properties required for the gas turbines components, such as lower thermal conductivity (i.e. 1.2 and 1.8 $Wm^{-1}K^{-1}$) (5), high thermal expansion coefficient (~$11x10^{-6}$ $°C^{-1}$), high compliance and strain tolerance (11,12). However, if the number of defects is too high, the mechanical properties of the coating are affected, making it susceptible to delamination by mechanisms such as erosion produced by foreign object damage (FOD), compromising the integrity of the components (13).

The number of defects in a TC must be controlled to maintain a balance between good thermal, mechanical and thermomechanical properties, ensuring the durability of the TBC system. There are several methods to control microstructure and TC defects, among them are the type of morphology of the raw material (crushed or spheroidized), and the spraying parameters such as gas mixture (Ar + He or H_2), gas flow and powder feed rate (14). Also, an alternative deposition process named suspension plasma spray (SPS) may be used to obtain a columnar microstructure, and a post-deposition process such as laser glazing helps control the quantity of defects across the TC, increasing the thermomechanical properties and hot corrosion resistance produced by CMAS or V_2O_5 (15–19). However, these alternatives require special and expensive equipment, higher control in process parameters, and handling of special, hazardous or corrosive reagents, requiring high investment in time and money to be easily implemented by the coating industry for the spraying of a component or in research by scientists dedicated to the spraying of TBC systems.

On the other hand, employing sensors that measure temperature and particle speed during spraying

doi: 10.25100/iyc.v28i1.14980

is a technically and economically viable option for precise control of the spraying parameters, as well as the lifetime of spray gun components. In this work, the design of experiments (DOE) methodology was systematically applied to optimize the parameters for the deposition of Yttria-Stabilized Zirconia (YSZ) coatings onto Inconel 625 using the Atmospheric Plasma Spray (APS) process. This rigorous approach allowed for the comprehensive exploration of the electric arc current and the hydrogen flowrate, measuring the changes in particle temperature and speed, determining their individual and collective effects on the coating's properties, such as morphology, defects (pores and cracks), crystal structure and thermal shock resistance.

Experimental Details

YSZ (Metco 204 NS-G, Oerlikon Metco) and NiCoCrAlY (Amdry 386-2.5,Oerlikon Metco) powders were used to apply the TC and BC, respectively, onto Inconel 625 substrate. The particle size distribution of the powders was determined using a Malvern Master Sizer 2000 analyzer and is shown in Figure 1. The Amdry 386-2.5 powder particles (Figure 1a) have spheroidal morphology with characteristic irregularities of the gas atomization process, with a particle size distribution of d (0.1) = 28.18 µm, d (0.5) = 40.07 µm, d (0.9) = 56.65 µm. On the other hand, the Metco 204 NS-G powder (Figure 1b) is composed of small particles within a spherical shell. The shell's size distribution is described by the manufacturers d (0.1) = 21.71 µm, d (0.5) = 53.31 µm, d (0.9) = 94.26 µm

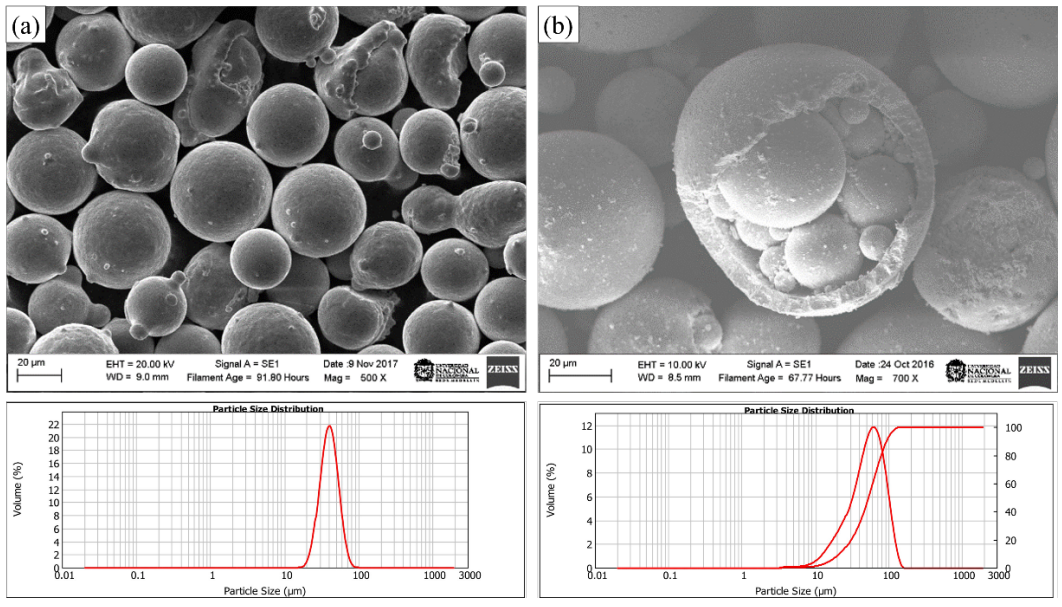

Figure 1. Morphology and particle size distribution of the powders used for BC and TC spraying. a) BC: Amdry 386-2.5, b) TC: Metco 204 NS-G. SEM.

The deposition process was carried out using a Sinplex Pro APS gun (Oerlikon Metco). Previous to the deposition the surface of the substrate was sandblasted with aluminum oxide (corundum F24) obtaining average roughness values of Ra = 4.58 ± 0.51µm, Rq = 5.78 ± 0.73 µm and Rz = 34.85 ± 3.43 µm. Afterwards, the samples were ultrasonically cleaned in isopropyl alcohol and dried

doi: 10.25100/iyc.v28i1.14980

with warm air. The spraying parameters for the NiCoCrAlY BC are presented in Table 1. An average thickness of 120 µm was obtained by using Argon and Helium as the main and secondary plasma gases, respectively.

Table 1. Spraying parameters for NiCoCrAlY BC.

Parameter	Unit of Measure	Value
Electric Arc Current	(A)	400
Main plasma gas Flowrate (Ar)	(NLPM)	80
Secondary plasma gas flowrate (He)	(NLPM)	70
Spraying Distance	(mm)	113
Spraying Speed	(mm/min)	1000
Powder flowrate	(g/min)	21

To determine the best deposition parameters of the TC, a 3^2 factorial design with 3 replicates was used. The electric arc current and the secondary plasma gas (H_2) flowrate were the factors considered in the experiment, while the rest of parameters were kept constant. The experimental sequence and the levels of the factors are observed in Table 2, where the response variables considered in the experiment were the temperature and the speed of the particles in flight.

Table 2. Factors and levels used in the factorial design for deposition of the TC. The following parameters were kept constant: main plasma gas flowrate (Ar)=50 NLPM, spraying distance=105 mm, spraying speed=1000 mm/min, powder flowrate=20 g/min.

Run Order	Electric Arc Current [A]	H_2 Flowrate [NLPM]
M1	370	9
M2	430	7
M3	370	5
M4	400	5
M5	370	9
M6	400	7
M7	370	7
M8	370	5
M9	430	7
M10	400	9
M11	430	9
M12	430	9
M13	400	9
M14	430	5
M15	400	7
M16	430	9
M17	400	9

doi: 10.25100/iyc.v28i1.14980

M18	370	5
M19	370	7
M20	430	7
M21	430	5
M22	400	5
M23	430	5
M24	400	7
M25	370	9
M26	400	5
M27	370	7

The response variables were measured with the aid of an AccuraSpray system (Tecnar) with a precision of 97.5% for the temperature and 99.5% for the speed. The data obtained from the equipment were processed with the Minitab 17 software. Figure 2 shows the Accuraspray system interface used for capturing data from the particles in flight. The red lines over the plasma jet shown in Figure 2a determine the region in which the measurement of the temperature and speed of the particles was carried out. This region was fixed for all the experiments to ensure that the measurements were useful to establish correlations with the morphology and microstructure of the coatings. The red line in Figure 2a is also used to adjust the angle of the plasma jet. This angle is produced by the flow of the powder carrier gas and the mass of the particles entering the jet radially at the SinplexPro gun.

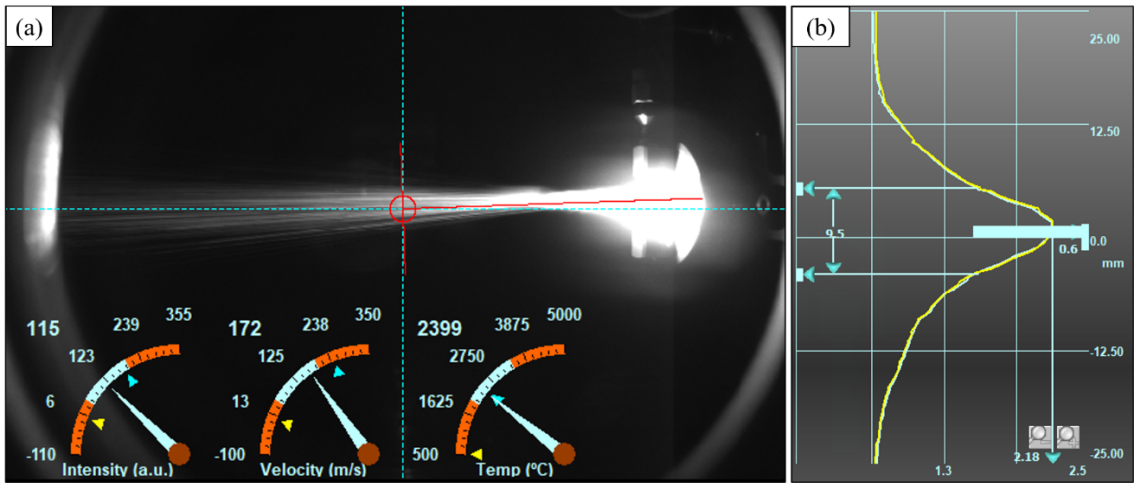

Figure 2. Data acquisition of temperature and speed of in-flight particles. Spraying parameters: 430 A and 5 NLPM of H_2. a) Measurement view of particles in flight, b) Plasma jet intensity graph.

Figure 2b shows the intensity profile across a section of the jet. The intensity profile allows determining the spot size of the plasma jet for a specific spraying condition, which is defined as the area that presents 70% of the maximum intensity recorded. For the spraying conditions shown in Figure 2, the plasma jet hits the substrate with a spot size with a diameter of 9.6 mm. The intensity profile of the spraying in process, represented by the blue curve, overlaps with the reference profile in yellow. This state was reached for the repetitions of each one of the evaluated spraying conditions; in this way, the repeatability of the experimental procedure was guaranteed.

doi: 10.25100/iyc.v28i1.14980

The cross-section of each sample was prepared following the ASTM E1920 standard (Standard Guide for Metallographic Preparation of Thermally Sprayed Coatings). The porosity quantification was carried out using digital image analysis following the ASTM E2109 standard (Standard Test Methods for Determining Area Percentage Porosity in Thermal Sprayed Coatings) and using ImageJ software. The images for the digital image processing were acquired using a Nikon eclipse LV 1000 microscope. Scanning Electron Microscopy (SEM) was used for the morphological characterization of the samples. The microscopes used were the Carl Zeiss EVO MA10 equipped with an EDS X-Act (Oxford Instruments), 129eV (nominal area 10 mm^2) solid state detector with SATW window and the JEOL JSM-5910LV equipped with an EDS Pentafet 7324 detector (Oxford Instruments), 133eV (nominal area 10 mm^2) with ATW2 window. Microstructural characterization was achieved with X-ray diffraction using a Panalytical EMPYREAN equipment with Bragg Brentano geometry, Cu-Kα radiation (λ = 1.5406 Å) and a measurement range between 20 and 80° with 0.01° step. Phase quantification was done by the Rietveld method using Xpert High Score Plus software. The crystallographic information to carry out the refinement was obtained from the ICDD charts number 01-082-1241 and 01-078-0047 for the tetragonal phase and the monoclinic phase, respectively. The background was fitted using Chebyschev polynomials and the peak profiles were fitted using a convolution of a Pseudo-Voigt and asymmetry function. In all cases the data fitted were adjusted to Chi^2 values below 3.

Cyclic thermal shock tests were performed using an electric furnace operating in air atmosphere. Each cycle consisted of heating the samples and holding them for 5 minutes at 1020°C, followed by direct cooling in water at room temperature. The failure criterion adopted was the detachment of more than 20% of the YSZ coating from the surface.

Results and Discussion

Temperature and speed of in-flight particles during top coating manufacturing

The assumptions of normality and constant variance for the in-flight particles speed and temperature were verified through the normal probability plots and the graphs of residuals vs. predicted values. The normal probability plot for the particles in flight speed is presented in Figure 3a. The residuals fit in a straight line, which validates the normal distribution assumption for the experiment. Moreover, the plot of residuals vs. predicted shows a random dispersion of the residuals with a mean value proximally zero, which validates the assumption of constant variance of the experiments. These facts were also verified in the graphs of normal probability and residuals vs. predicted for the temperature of the in-flight particles (Figure 3b). It was then verified the correct randomization of the tests and the absence of operational biases in the experimental plan.

doi: 10.25100/iyc.v28i1.14980

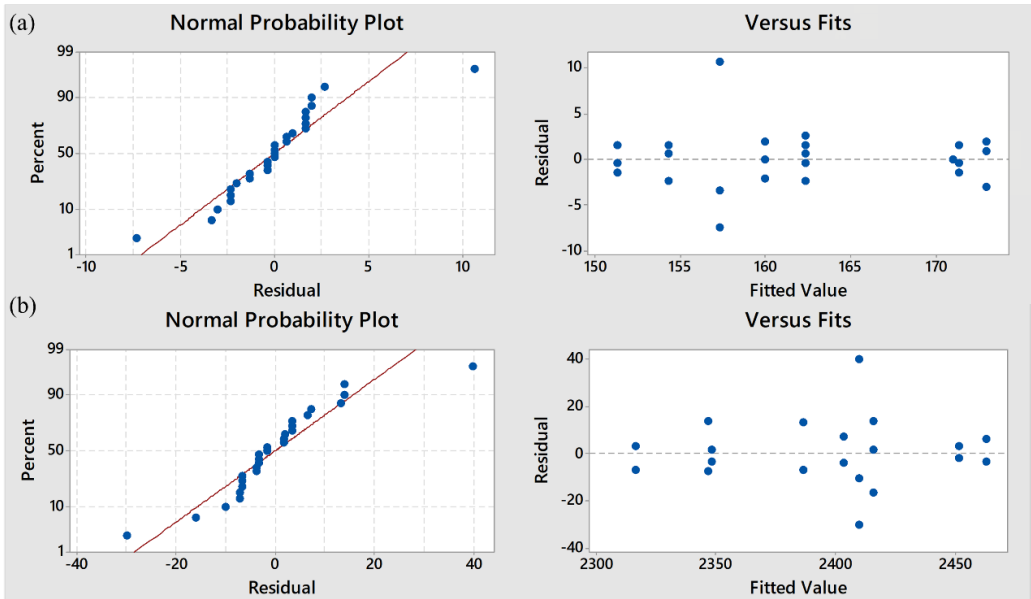

Figure 3. Normal probability and fitted value graphs for the Speed (a) and the Temperature (b) of the particles in flight.

The factorial design analysis of variance (ANOVA) of the two response variables is shown in Table 3. A p-value < 0.05 is observed for the influence of the electric arc current on the speed and temperature of the in-flight particles, which indicates that this factor has an important effect on both response variables. On the other hand, a p-value <0.05 is observed for the influence of the hydrogen flowrate on the temperature of the in-flight particles, and a p-value = 0.266 for the influence of the hydrogen flowrate on the speed of the particles. These results indicate that the hydrogen flowrate only has a substantial effect on the temperature of the particles and does not present a significant effect on their speed during the thermal spraying process in the experimental region evaluated in this work. It should also be noted that the combined effect of the hydrogen flowrate and the electric arc current did not present a major effect on the speed and temperature of the particles in flight, since p-values > 0.05 were obtained.

Table 3. Analysis of variance of the experimental data

	Speed	**Temperature**
Parameter	**p-value**	**p-value**
Electric Arc Current	0.000	0.000
H_2 Flowrate	0.266	0.000
Electric Arc Current - H_2 Flowrate	0.645	0.092

The effect of the electric current and H_2 flowrate on the speed and temperature of in-flight particles is observed in Figure 4. Figure 4a shows how an increase in the electric arc current from 370 to 430 A produces an increase in the particle speed of 20 m/s keeping the hydrogen flowrate at 5

doi: 10.25100/iyc.v28i1.14980

NLPM, and of 16 m/s for a hydrogen flowrate of 9 NLPM. The low dispersion of the acquired data is evident from the absence of overlapping of the error bars for the three levels of electric arc current evaluated. This emphasizes the importance of the effects suggested by the p-values obtained through the ANOVA analysis (Table 3). The observed increase in the particles' speed is due to the reduction of the density of the plasma with the increase of the enthalpy (20). In addition, the influence of the H_2 flowrate and its combined effect with the electric arc current on the speed of the particles were not significant, presenting a difference in the mean values that did not exceed 5 m/s with the increase in the hydrogen flowrate at a constant current value (Figure 4a).

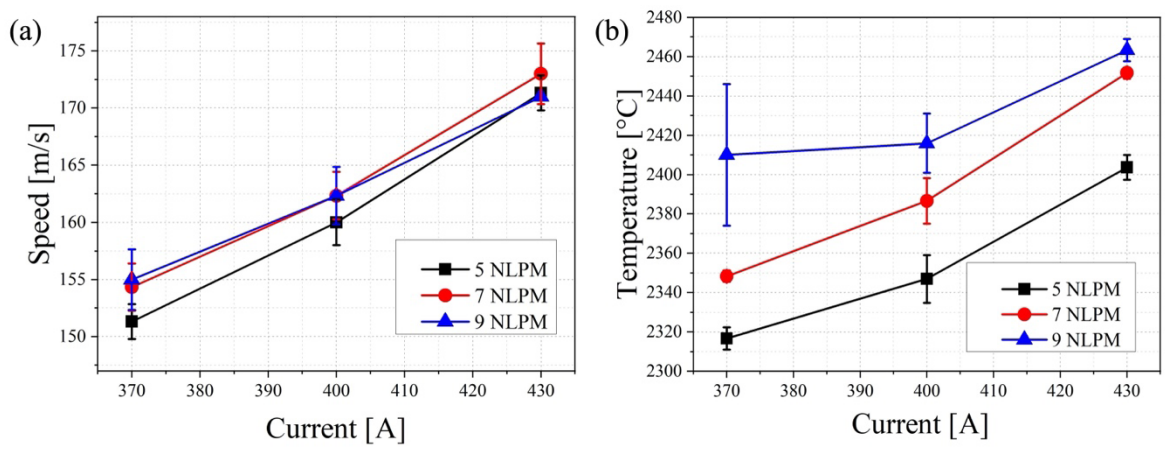

Figure 4. Effects of the Hydrogen flowrate and electric arc current on the speed (a) and temperature (b) of the in-flight particles.

For the case of the temperature of the in-flight particles, the assessed factors had a significant effect on this response variable, as can be seen in Figure 4b. Increases of up to 103°C occurred for the different H_2 flowrates and electric current combinations. This is because the electric arc current increases the enthalpy due to increased ionization. In the case of H_2 flowrate, H_2 dissociation produces high energy in the form of heat due to its diatomic state. In addition, the increase in the H_2 content leads to a reduction in the plasma electrical conductivity, increasing the voltage and power of the system (20).

YSZ morphology and microstructure

Figure 5 shows the cross section of the TBC systems sprayed under different conditions. During the BC spraying, the powder particles reached a speed of 320 m/s. The thickness of the BC was 123.13 ± 9.99 µm, the average porosity was 8.9 ± 3.7%, and the percentage of oxides was 4.6 ± 1.5%. The low dispersion of data indicates a high repeatability of the BC manufacturing process with the spraying parameters implemented. YSZ morphology, on the other hand, varies significantly with the H_2 flowrate. An increase in thickness and a decrease in porosity of the ceramic layer were observed when the H_2 flowrate increased. Higher values of electric arc current produced the same effect on the porosity and the thickness of the TC as shown in Figure 6.

doi: 10.25100/iyc.v28i1.14980

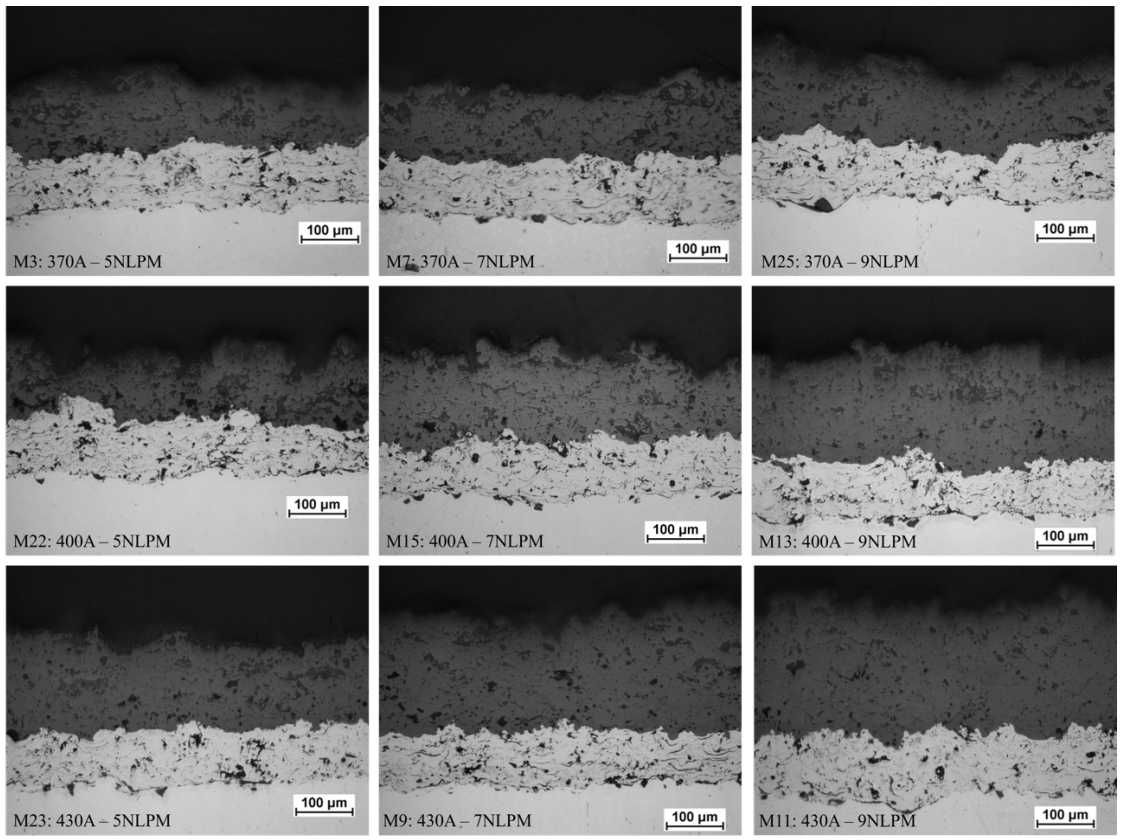

Figure 5. BC (NiCoCrAlY) and TC (YSZ) microstructure for different spraying conditions. LOM.

Considering the high temperatures produced by these deposition parameters, the particles in flight will mostly be in a molten or semi-molten state. This will have a mitigating effect the rebound effects upon substrate impact. Consequently, a greater quantity of powder particles is satisfactorily deposited, resulting in thicker ceramic layers. This elevation in in-flight particles temperature, coupled with heightened average speed, facilitates particle deformation upon substrate impact, fostering the formation of flatter splats and thereby reducing porosity.

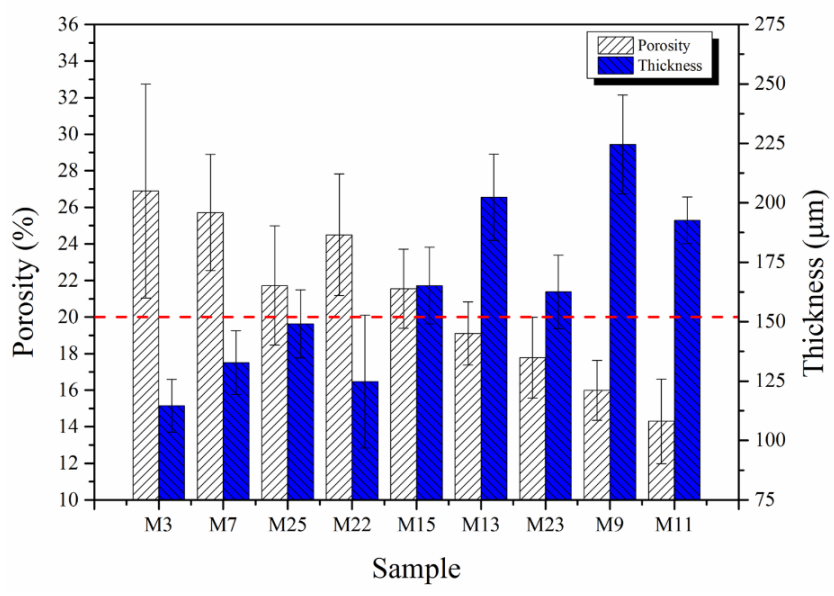

Figure 6. Porosity and thickness of the as-sprayed coatings

doi: 10.25100/iyc.v28i1.14980

Figure 6 shows that only M9, M11, M13 and M23 samples have an average porosity lower than 20%. These samples also presented greater thickness with values of 224.5, 192.6, 202.3 and 162.5 µm, respectively. A larger gradient of temperature is achieved during operation for higher thickness of the ceramic layer, which improves the protection against high temperatures of the components of the hot gas path of thermoelectric generation turbines due to the increase in the insulating effect of the TC. Porosity levels superior to 20% (M3, M7, M22, M25 and M15) lead to the lessening of the mechanical properties, which compromises the integrity of the turbine when it is in operation. Consequently, samples with porosity higher than 20% were discarded for further characterization.

Figure 7 shows the X-Ray diffraction results for YSZ powder as well as for M9, M11, M13 and M23 coated samples. All the samples present a high intensity without a substantial variation of the peak 2θ = 30.1° of the (101) plane of the tetragonal phases t'-YSZ and t-YSZ. These phases also present peaks at 2θ = 73.2° and 74.1° which correspond to the (004) and (400) planes of the t'-YSZ phase, as well as the (004) plane of the t-YSZ phase at 2θ = 74.4° (21). Furthermore, peaks for ($\bar{1}$11) and (111) planes of the monoclinic phase (m-ZrO_2) were observed at angles 2θ = 28.1° and 31.4°, respectively. Phase quantification using Rietveld analysis (table 4) confirmed that all the as-sprayed samples have more than 90 wt. % of tetragonal phase (t'-YSZ + t-YSZ), which is desirable for thermal barrier applications since this phase is responsible for the good thermo-mechanical properties of the TBC system (22–24). A reduction of t'-YSZ phase was observed after spraying, which stabilized a bigger amount of t-YSZ phase, and reduced the amount of m-ZrO_2 phase.

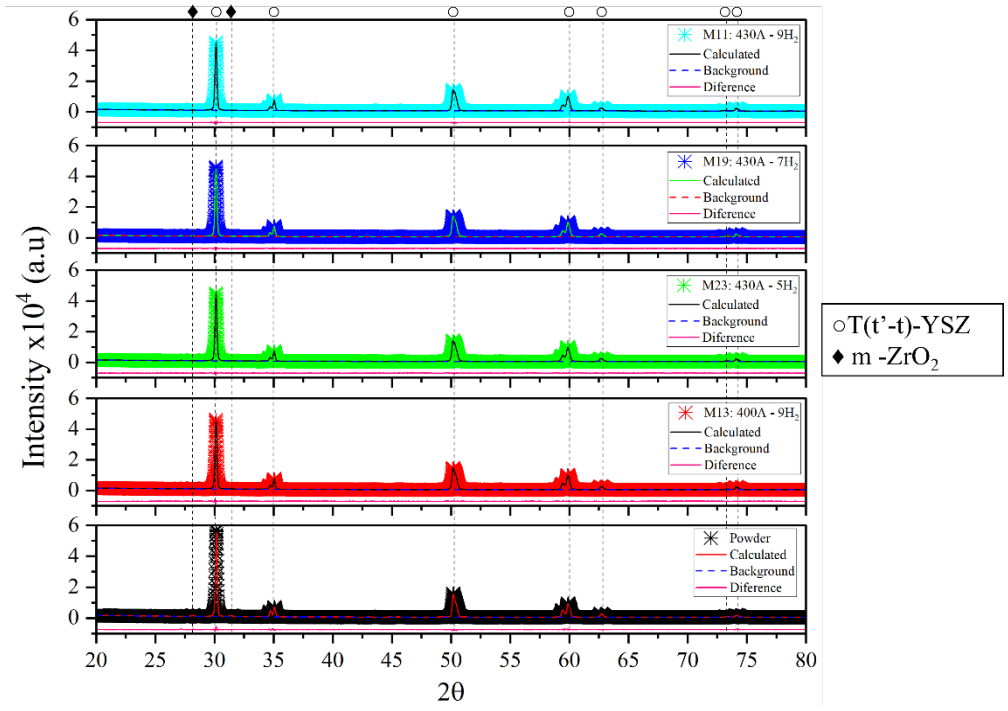

Figure 7. X Ray Diffractograms for power, M9, M11, M13 and M23 samples.

doi: 10.25100/iyc.v28i1.14980

Table 4. Phase percentages using the Rietveld method.

Sample	t'-YSZ	t-YSZ	m-ZrO_2
Powder 204NS-G	84.4	4.89	10.7
M13: 400A-9 NLPM H_2	82.5	10.1	7.5
M23: 430A-5 NLPM H_2	81.5	10.4	8.1
M9: 430A-7 NLPM H_2	81.6	10.9	7.5
M11: 430A-9 NLPM H_2	82.3	10.6	7.1

The results indicated that the electric arc current and H_2 flowrate had negligible impact on the crystalline structure of the YSZ coatings. In all the samples the proportions of t'-YSZ, t-YSZ and m-ZrO_2 phases remained comparable, with relative variations of less than 1 wt. %. According to these results, the samples comply with a percentage of tetragonal phase (T) greater than 90 wt. %.

Thermal shock resistance

The resistance to thermal shock of the sample M9 (430 A-7 NLPM H_2) was evaluated since it presented the best values of thickness and porosity. Figure 8 shows the changes in the mass of sample M9 as a function of the number of thermal shock cycles.

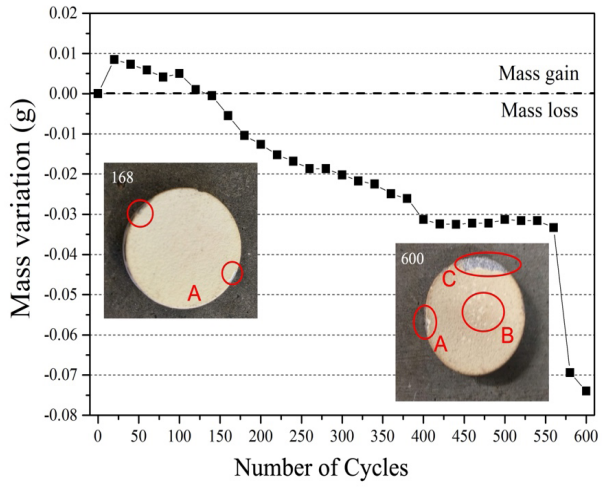

Figure 8. Mass variation with number of cycles in thermal shock experiments. A = Edge Delamination, B = Exfoliation, and C = Delamination. Sample M9 (430 A – 7 NLPM H_2).

doi: 10.25100/iyc.v28i1.14980

An increase in the mass of the samples due to oxidation of the substrate and BC was verified (25). From the 168th cycle on the sample presented mass losses caused by delamination at the edges (see detail A in Figure 8). At the end of the test (600 cycles), the sample presented 6.6% delamination of the coating and exfoliation (detail B). However, this was not a cause for discarding the sample following the criterion of 20% of the delaminated area. Other YSZ TBC systems tested under the same conditions (25,26) showed discardable system failures after 220 and 417 cycles, while more shock-resistant coatings such as CYSZ TBC systems failed at the 307th cycle and bilayer systems at the 60th cycle (27,28). This indicates that the selected spraying conditions led to a higher strength comparable with several literature reports**.**

Figure 9a shows the surface of the M9 sample (430 A – 7 NLPM H_2) after 600 cycles, where the coating's exfoliation is evidenced as a result of the generation and propagation of cracks due to TC defects that produced a loss in thickness of the coating. The cross section in Figure 9b shows that the delamination of the TBC system occurred at the BC/TC interface. This is because the stresses generated by the difference between the coefficients of thermal expansion of the BC and the TC produce cracks that coalesce and, combined with the coating's imperfections, propagate and produce rupture of the TGO followed by delamination and later TBC system failure (25,29). Figure 9c shows the formation of a highly undulated TGO with a thickness of 2.62 ± 0.57 µm, spinels (Ni/Co/Cr oxides - light gray areas near the TGO) (30) and the depletion of the β phase (AlNi). The latter is due to the diffusion of aluminum towards the surface of the BC because of the thermal exposure, which reacts with oxygen from the environment and forms the TGO (25). As the thermal exposure continues, more of the Aluminum diffuses towards the surface, reducing the internal β phase of the coating.

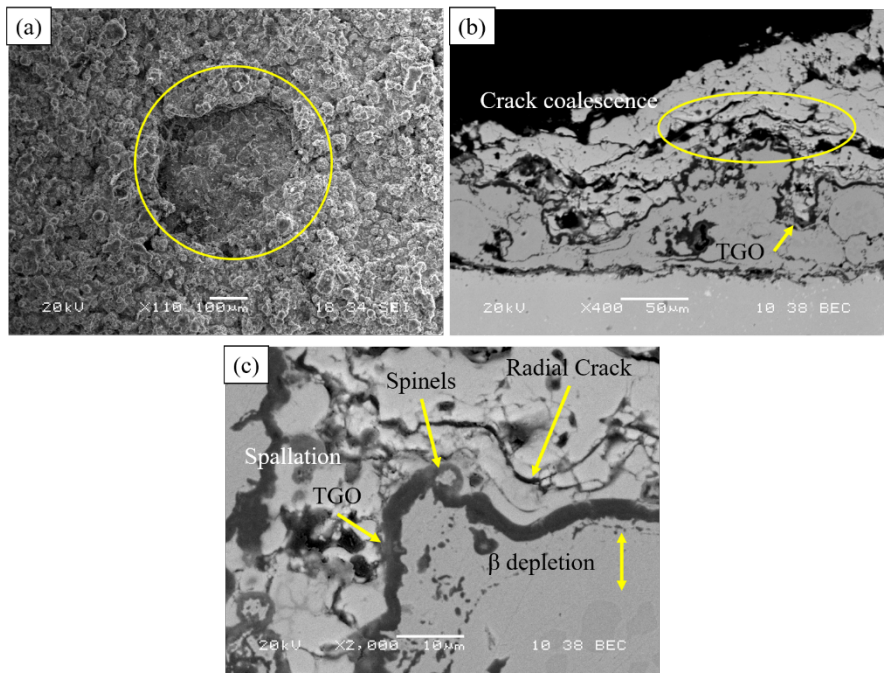

Figure 9. M9 Sample after 600 thermal shock cycles. (a) Exfoliated surface, (b) Cross Section of the failure area at 400X, (c) Cross Section of the failure area at 2000X. SEM

doi: 10.25100/iyc.v28i1.14980

Conclusions

The deposition parameters of YSZ coatings applied onto Inconel 625 alloy by Atmospheric Plasma Spraying were determined experimentally through a Design of Experiments (DOE) methodology. The speed of the in-flight particles presented high dependence on the electric arc current but not on the hydrogen flowrate. The temperature of the particles, on the other hand, showed strong correlation with these two variables.

The coatings with the best characteristics in terms of the percentage of tetragonal phase (> 90 wt.%), porosity (15.9% and 14.3%), and thickness (224.5 and 192.6 µm) were obtained with the parameters 430 A - 7 NLPM H_2 and 430 A - 9 NLPM H_2, respectively.

The adequate selection of spraying parameters was supported by the results of thermal shock tests performed with the coating obtained with 430 A and 7 NLPM H_2, which showed a remarkable performance in comparison with reports from the literature, presenting a detached area of only 6.6% of the coating after 600 cycles.

Acknowledgements

The authors thank Empresas Públicas de Medellín – EPM and MINCIENCIAS for financial support through the projects n. CW264699 and CT 167-2021, respectively.

CrediT authorship contribution statement

Conceptualization - Ideas: Jhonattan de la Roche, José Alexander Arboleda, Lina María Chica Osorio y Alejandro Toro. Data curation: Jhonattan de la Roche y José Alexander Arboleda. Formal analysis: Jhonattan de la Roche, José Alexander Arboleda, Lina María Chica Osorio y Alejandro Toro. Investigation: Jhonattan de la Roche y José Alexander Arboleda. Methodology: Jhonattan de la Roche y José Alexander Arboleda. Project Management: Alejandro Toro. Resources: Alejandro Toro. Supervision: Lina María Chica Osorio y Alejandro Toro. Validation: Lina María Chica Osorio y Alejandro Toro. Writing - original draft - Preparation: Jhonattan de la Roche y José Alexander Arboleda. Writing - revision and editing -Preparation: Jhonattan de la Roche, José Alexander Arboleda, Lina María Chica Osorio y Alejandro ToroFinancing: does not declare.

Conflict of interest: does not declare. Ethical aspect: does not declare.

References

1. Chen L, Li B, Feng J. Rare-earth tantalates for next-generation thermal barrier coatings. Prog Mater Sci. 2024;144:101265. https://doi.org/10.1016/j.pmatsci.2024.101265

2. Sezavar A, Sajjadi SA. A review on the performance and lifetime improvement of thermal barrier coatings. J Eur Ceram Soc. 2025;45:117274. https://doi.org/10.1016/j.jeurceramsoc.2025.117274

doi: 10.25100/iyc.v28i1.14980

3. Chen L, Li B, Feng J. Rare-earth tantalates for next-generation thermal barrier coatings. Prog Mater Sci. 2024;144:101265. https://doi.org/10.1016/j.pmatsci.2024.101265

4. Lokachari S, Leng K, Rincon Romero A, Curry N, Brewster G, Norton A, Hussain T. Processing-Microstructure-Properties of Columns in Thermal Barrier Coatings: A Study of Thermo-Chemico-Mechanical Durability. ACS Appl Mater Interfaces. 2024;16:10646-10660. https://doi.org/10.1021/acsami.3c16681

5. Mehboob G, Liu M-J, Xu T, Hussain S, Mehboob G, Tahir A. A review on failure mechanism of thermal barrier coatings and strategies to extend their lifetime. Ceram Int. 2020;46:8497-8521. doi: https://doi.org/10.1016/j.ceramint.2019.12.200

6. Leng K, Romero AR, Curry N, Hussain T. Multilayer GZ/YSZ thermal barrier coating from suspension and solution precursor plasma spray. Ceram Int. 2024;50:631-649. https://doi.org/10.1016/j.ceramint.2023.10.142

7. Gómez JA, de la Roche J, Gómez P, Toro A. Influence of Iron Oxide Deposits on the Hot Corrosion Resistance of YSZ Thermal Barrier Coatings in Molten Vanadium Pentoxide. Materials and Corrosion. 2025; https://doi.org/10.1002/maco.202414673

8. Jiang C, Hao W, Liu C, Shi D, Song W. Thermal cycling performance of GYbZ/YSZ thermal barrier coatings with different microstructures based on finite element simulation. J Alloys Compd. 2025;1010:177185. https://doi.org/10.1016/j.jallcom.2024.177185

9. Vagge ST, Ghogare S. Thermal barrier coatings: Review. Mater Today Proc. 2022;56:1201-1216. https://doi.org/10.1016/j.matpr.2021.11.170

10. Fu Y, Yao Z, Chen Y, Wang H, Li Y, Dong J. Progress in the Deposition Mechanisms and Key Performance Evaluation of Thermal Barrier Coatings for Turbine Blades: A Review. Acta Metallurgica Sinica (English Letters). 2025;38:177-204. https://doi.org/10.1007/s40195-024-01799-6

11. Clarke DR, Oechsner M, Padture NP. Thermal-barrier coatings for more efficient gas-turbine engines. MRS Bull. 2012;37:891-898. https://doi.org/10.1557/mrs.2012.232

12. Padture NP, Gell M, Jordan EH. Thermal Barrier Coatings for Gas-Turbine Engine Applications. Science (1979). 2002;296:280-284. https://doi.org/10.1126/science.1068609

13. Darolia R. Thermal barrier coatings technology: critical review, progress update, remaining challenges and prospects. International Materials Reviews [Internet]. 2013;58:315-348. https://doi.org/10.1179/1743280413Y.0000000019

doi: 10.25100/iyc.v28i1.14980

14. Jiang XY, Hu J, Jiang SL, Wang X, Zhang LB, Li Q, Lu HP, Yin LJ, Xie JL, Deng LJ. Effect of high-enthalpy atmospheric plasma spraying parameters on the mechanical and wear resistant properties of alumina ceramic coatings. Surf Coat Technol. 2021;418:127193. https://doi.org/10.1016/j.surfcoat.2021.127193

15. Lokachari S, Leng K, Rincon Romero A, Curry N, Brewster G, Norton A, Hussain T. Processing-Microstructure-Properties of Columns in Thermal Barrier Coatings: A Study of Thermo-Chemico-Mechanical Durability. ACS Appl Mater Interfaces. 2024;16:10646-10660. https://doi.org/10.1021/acsami.3c16681

16. Kebriyaei A, Rahimipour MR, Razavi M. Solution Medium Suspension Plasma Spray (SMSPS): A Microstructure and High-Temperature Properties Analysis of YSZ Thermal Barrier Coating. Journal of Thermal Spray Technology. 2024;33:2395-2407. https://doi.org/10.1007/s11666-024-01848-7

17. Tsai PC, Hsu CS. High temperature corrosion resistance and microstructural evaluation of laser-glazed plasma-sprayed zirconia/MCrAlY thermal barrier coatings. Surf Coat Technol. 2004;183:29-34. https://doi.org/10.1016/j.surfcoat.2003.08.090

18. Pakseresht AH, Kimiayi A, Alizadeh M, Nuranian H, Faeghinia A. Microstructural study and hot corrosion behavior of bimodal thermal barrier coatings under laser heat treatment. Ceram Int. 2020;46:19217-19227. https://doi.org/10.1016/j.ceramint.2020.04.259

19. Avci A, Karaba M, Akdo an Eker A, Akman E, Aslan C. Hot corrosion behavior of CYSZ thermal barrier coating with optimized laser surface modification. Ceram Int. 2023;49:31396-31404. https://doi.org/10.1016/j.ceramint.2023.07.087

20. Schneider KE, Belashchenko V, Dratwinski M, Siegmann S, Zagorski A. Thermal Spraying for Power Generation Components. WILEY-VCH. Weinheim: WILEY-VCH Verlag GmbH & Co.; 2006. https://doi.org/10.1002/3527609342

21. Witz G, Shklover V, Steurer W, Bachegowda S, Bossmann H. Phase evolution in yttria stabilized zirconia thermal barrier coatings studied by rietveld refinement of X ray powder diffraction patterns. Journal of the American Ceramic Society. 2007;90:2935-2940. https://doi.org/10.1111/j.1551-2916.2007.01785.x

22. De la Roche J, Gómez PA, Alvarado-Orozco JM, Toro A. Hot corrosion and thermal shock resistance of Dense-CYSZ/YSZ bilayer thermal barrier coatings systems applied onto Ni-base superalloy. J Eur Ceram Soc. 2020;0-1. https://doi.org/10.1016/j.jeurceramsoc.2020.07.004

23. De la Roche J, Alvarado-Orozco JM, Toro A. Hot corrosion mechanism of yttria-stabilized zirconia powder in the presence of molten Na2SO4 + V2O5 salts. Rare Metals. 2021;40:1307-1316. https://doi.org/10.1007/s12598-020-01388-3

doi: 10.25100/iyc.v28i1.14980

24. De la Roche J, Alvarado-Orozco JM, Gómez PA, Cano IG, Dosta S, Toro A. Hot corrosion behavior of dense CYSZ/YSZ bilayer coatings deposited by atmospheric plasma spray in Na2SO4 + V2O5 molten salts. Surf Coat Technol. 2022;432:128066. . https://doi.org/10.1016/j.surfcoat.2021.128066

25. Khan AN, Lu J. Behavior of air plasma sprayed thermal barrier coatings, subject to intense thermal cycling. Surf Coat Technol. 2003;166:37-43. https://doi.org/10.1016/S0257-8972(02)00740-5

26. Jamali H, Mozafarinia R, Razavi RS, Ahmadi-Pidani R. Comparison of thermal shock resistances of plasma-sprayed nanostructured and conventional yttria stabilized zirconia thermal barrier coatings. Ceram Int. 2012;38:6705-6712. https://doi.org/10.1016/j.ceramint.2012.05.060

27. Nejati M, Rahimipour MR, Mobasherpour I, Pakseresht AH. Microstructural analysis and thermal shock behavior of plasma sprayed ceria-stabilized zirconia thermal barrier coatings with micro and nano Al2O3 as a third layer. Surf Coat Technol. 2015;282:129-138. https://doi.org/10.1016/j.surfcoat.2015.10.030

28. Ahmadi-Pidani R, Shoja-Razavi R, Mozafarinia R, Jamali H. Improving the thermal shock resistance of plasma sprayed CYSZ thermal barrier coatings by laser surface modification. Opt Lasers Eng. 2012;50:780-786. https://doi.org/10.1016/j.optlaseng.2011.12.007

29. Evans AG, Mumm DR, Hutchinson JW, Meier GH, Pettit FS. Mechanisms controlling the durability of thermal barrier coatings. Prog Mater Sci. 2001;46:505-553. https://doi.org/10.1016/S0079-6425(00)00020-7

30. Rabiei A, Evans AG. Failure mechanisms associated with the thermally grown oxide in plasma-sprayed thermal barrier coatings. Acta Mater [Internet]. 2000;48:3963-3976. https://doi.org/10.1016/S1359-6454(00)00171-3

doi: 10.25100/iyc.v28i1.14980